Probing the Fermi surfaces of coupled double quantum wells in the presence of an in-plane magnetic field

1997 J. Phys.: Condens. Matter 9 1079

(http://iopscience.iop.org/0953-8984/9/5/013)

J. Phys.: Condens. Matter **9** (1997) 1079–1094. Printed in the UK PII: S0953-8984(97)78782-4

Probing the Fermi surfaces of coupled double quantum wells in the presence of an in-plane magnetic field

I S Millard†, N K Patel‡, C Foden‡, E H Linfield†, D A Ritchie†, G A C Jones† and M Pepper†‡

† Cavendish Laboratory, University of Cambridge, Madingley Road, Cambridge CB3 OHE, UK
‡ Toshiba Cambridge Research Centre, 260 Science Park, Milton Road, Cambridge CB4 4WE, UK

Received 18 October 1996

Abstract. The anticrossing of the dispersion relations of two two-dimensional electron gases (2DEGs) in an in-plane magnetic field results in distorted Fermi surfaces, leading to density of states and effective mass changes. We have used two different techniques to probe such changes with both the in-plane field and carrier density being systematically altered. The first technique uses a fixed perpendicular field to form Landau levels. By following the evolution of these Landau levels with in-plane field, carrier density and temperature, we are able to determine changes in the subband populations and effective masses. The second technique uses a third conducting layer as a detector of chemical potential changes in the coupled electron gases. This method also allows the determination of effective mass changes in an in-plane field. Calculations of the dispersion curves have been made, illustrating the effect of the parallel field upon subband occupancy and effective mass. These calculations are compared with the experimental data from both methods and are found to be in good agreement.

1. Introduction

Coupled two-dimensional electron gases (2DEGs) have revealed a wide range of new physical phenomena. In weakly coupled devices, where significant coupling of the two 2DEGs occurs only at the point of matched carrier densities, studies have been made upon resistance resonances [1], resonant tunnelling [2] and the Coulomb gap [3] to tunnelling at high magnetic fields. In more strongly coupled structures, there has been much theoretical [4, 5] and experimental [6–8] work on the quantum Hall effect, as well as studies using parallel magnetic fields ($B_{\|}$) [9–11]. The effect of a parallel field is to change the relative canonical momentum $\hbar k$ of the 2DEGs within each confining quantum well (QW). As $B_{\|}$ is increased, the dispersion curves for each QW are separated in momentum space and, in the presence of coupling, anticross. This creates a partial energy gap that (i) causes van Hove singularities in the density of states at the gap edges, (ii) changes the occupancy of the subbands [12] and (iii) changes the electrons' effective mass.

Previous work has investigated the in-plane field dispersions of coupled 2DEG systems at resonance [11, 13] by tilting the sample and then varying a magnetic field. Analysis of the Shubnikov–de Haas (SdH) oscillations enabled subband densities and effective masses to be determined. In this technique, both the parallel and perpendicular magnetic field components are changed simultaneously. In order to avoid this, we use a gate bias to change the subband densities at *fixed* tilt angles and magnetic fields. Thus we are able to

0953-8984/97/051079+16$19.50

alter, independently, the perpendicular and parallel magnetic field components and measure over a wide range of carrier densities. Our data enable us to map out the population and depopulation of the subbands as a function of both parallel field and gate bias. Theoretically, the two subbands should have different behaviour with in-plane field [10]. One subband should show an increasing effective mass with parallel field and the other a decreasing effective mass. Whereas previous work has probed the smaller-effective-mass subband, at resonance, in our sample only the larger-effective-mass subband is occupied for a wide range of gate voltages and parallel fields. We therefore determine the larger effective mass for a wide range of gate biases.

In this study we use two experimental techniques to probe this system: the first uses a fixed perpendicular magnetic field to form Landau levels (LLs) and fixed in-plane field to distort the Fermi surfaces. By changing the gate bias, magneto-resistance oscillations were observed as the LLs were populated. Analysis of the magneto-transport data clearly showed how the parallel field changes the subband occupancy through the anticrossing of the two dispersion curves. The temperature dependence of the magneto-oscillations was also used to determine changes in the electrons' effective mass. The second technique employed a third conducting layer as a detector [14, 15]. This enabled us to measure the chemical potential changes in the strongly coupled 2DEGs and to determine the effective mass as a function of parallel field. In addition, unlike previous measurements of the effective mass, this method does not require the presence of Landau levels. Our results are finally compared with self-consistent calculations for the structure, which are seen to be in good agreement, confirming our interpretations of the effect of the parallel field upon the Fermi surface.

2. Samples and processing

The wafer used for this work was a GaAs–$Al_{0.33}Ga_{0.67}As$ heterostructure grown by molecular beam epitaxy on an undoped GaAs substrate. Electrons were confined to three GaAs quantum wells, which, from the surface downwards (see figure 1(a)), consisted of a strongly coupled pair of 95 and 120 Å width separated by a 25 Å $Al_{0.33}Ga_{0.67}As$ barrier, and a third 120 Å QW separated by a 200 Å $Al_{0.33}Ga_{0.67}As$ barrier. Carriers were supplied by modulation doped layers situated above and below the three QWs, with the three QW widths being chosen to ensure that all three layers were populated. Using optical lithography, a Hall bar mesa (see figure 1(b)), was defined using wet etching and ohmic contacts formed using AuGeNi. Schottky NiCr–Au surface gates enabled both independent contacts [16] to be made to the uncoupled lower 2DEG and also allowed the density of the strongly coupled 2DEGs to be varied. The densities in the strongly coupled subbands at zero applied gate bias were 1.44×10^{15} and 0.17×10^{15} m^{-2} with mobilities 22 and 28 m^2 V^{-1} s^{-1} for the first and second subbands respectively. The decoupled 2DEG had a density of 2.90×10^{15} m^{-2} and mobility of 40 m^2 V^{-1} s^{-1}. All of the data was taken at a temperature of 1.5 K using low-frequency ac lock-in techniques.

3. Experimental methods

The parallel ($B_\parallel$) and perpendicular ($B_\perp$) magnetic field components were controlled by mounting the sample at an angle to the applied field [9–11]. As a field sweep would, therefore, change both components simultaneously we chose to sweep the surface gate bias at fixed $B_\parallel$ and $B_\perp$. Note, however, that by changing the applied field and using a computer controlled *in situ* sample rotator to adjust the sample angle, both the

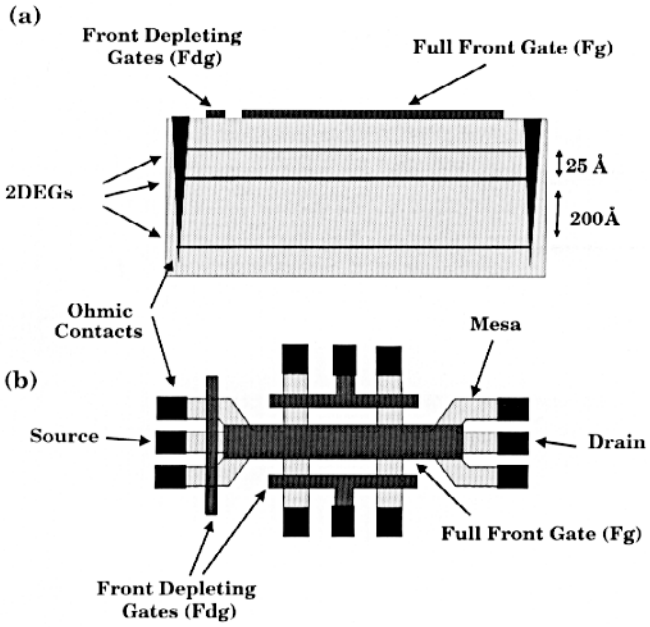

Figure 1. (a) The sample structure and the relative positions of the three 2DEGs and (b) the layout of the mesa, full front gate (Fg) and front depleting gates (Fdg) used for independently contacting the detector 2DEG.

parallel and perpendicular components may be adjusted independently. This technique was used in measurements of both the magneto-transport (subsection 3.1) and compressibility, (subsection 3.2). In the magneto-transport experiments all of the conducting layers were probed in parallel, with both the longitudinal and Hall resistances being measured. In contrast, for the compressibility measurements, independent contacts were made to the bottom, uncoupled, detector layer [15, 17, 18]. The carrier density of this layer was then determined from the low-$B_\perp$ Hall resistance.

3.1. Magneto-transport

In the presence of a quantizing perpendicular magnetic field, each subband develops into a series of LLs. If the structure is then depleted with a gate bias, the resistance will oscillate as the LLs are sequentially depopulated. These oscillations can be assigned to the different subbands and used to provide information upon the subband populations. The temperature dependence of the magneto-oscillations may also be used to determine the effective mass of the electrons. Using the *in situ* rotator, these measurements were made at different parallel fields whilst maintaining a constant perpendicular field.

The amplitude of the magneto-oscillations of a single subband is given by

$$A(B,T) = C[(2\pi^2 m^* k_B T/\overline{h}eB)/\sinh(2\pi^2 m^* k_B T/\overline{h}eB)]\mathrm{e}^{-(\pi/w_c\tau_{LL})} \qquad (1)$$

where C is a constant, m^* the effective mass, B the perpendicular field, T the temperature, w_c the cyclotron resonance frequency (eB/m^*) and k_B the Boltzmann constant. The Landau scattering lifetime τ_{LL} is assumed to be constant within the temperature range used. Experimentally, though, we are measuring the four-terminal longitudinal and transverse

(Hall) resistivities of two or more subbands in parallel. As, however, the conductivities of each subband are additive, the conductance *amplitude* of the magneto-conductance oscillations would be unaffected by the presence of other subbands. We therefore transform our data from resistivity (ρ) to conductivity (σ) via the inverse tensor relation $\sigma = \rho^{-1}$. If we consider the situation in which the perpendicular field is held constant and the gate voltage is made increasingly negative, the magneto-oscillations, due to the LLs, are then superimposed upon a decreasing background, which changes with both parallel field and subband population. The conductivity data are, therefore, filtered to remove the low-frequency (with respect to the magneto-oscillations) magneto-conductance background. This technique is very effective at removing the background whilst leaving the amplitude of the magneto-oscillations unchanged. The amplitude difference between adjacent maxima and minima was thus obtained for a number of different temperatures; typically twenty temperatures from 1.5 to 5 K were found to be sufficient. By normalizing the amplitude function (equation (1)) to a temperature T_0 (equation (2) below), a fitting procedure could be used to extract the effective mass [11].

$$A_N(B,T) = A(B,T)/A(B,T_0) = T\sinh(2\pi^2 m^* k_B T_0/\hbar eB)/T_0\sinh(2\pi^2 m^* k_B T/\hbar eB). \quad (2)$$

Repeating this procedure for different parallel fields enabled the effective mass ratio m^*/m_0, where m_0 is the electrons mass at zero $B_\parallel$, to be mapped out for a particular subband.

3.2. Compressibility

The device structure is composed of two strongly coupled 2DEGs (probed) above a decoupled 2DEG (detector), which may be contacted independently using surface gates [19]. By measuring the Hall voltage of the independently contacted detector layer at low perpendicular fields ($B_\perp < 0.3$ T), density changes due to the screening properties [15, 17] of the coupled 2DEGs may be determined. As shown in previous publications [15, 20] the measured density changes in the detector 2DEG (δN_d) may be related to the density changes within the probed layer (δN_p) by a capacitive relationship:

$$\delta N_d/\delta N_p = (\varepsilon/de^2)(\delta\mu_{KE}/\delta N_p + \delta\mu_H(N_p)/\delta N_p + \delta\mu_{xc}(N_p)/\delta N_p) \quad (3)$$

where d is the distance between the probe and detector layers, N_d and N_p refer to the detector and probed layer carrier densities respectively and ε is the effective dielectric constant. The chemical potential change $\delta\mu/\delta N_p$ has, therefore, three components: a positive, constant, kinetic energy component ($\delta\mu_{KE}$), a negative many-body exchange and correlation interaction term ($\delta\mu_{xc}$) and a negative Hartree term ($\delta\mu_H$) [17, 20]. The sign of the density change ($\delta N_d/\delta N_p$) will therefore depend upon the relative sizes of the three components, with the negative interactions dominating at low carrier densities and the positive kinetic energy component dominant at high densities [15].

Firstly it is necessary to convert gate voltage (V_g) into the density of the probed 2DEG (N_p). This can be achieved by taking gate sweeps of all three layers in parallel at different $B_\perp$ (with $B_\parallel = 0$), and analysing the resulting magneto-oscillations. The deduced gate voltage–density relation was $N_p = 8.612V_g + 2.186(10^{15}\ \mathrm{m}^{-2})$. Using the high-density limit, we can relate the density changes to the kinetic energy term, as given by $\delta\mu_{KE}/\delta N_p = \pi\hbar^2/m^*$. Previous measurements [21] upon double-layer systems have shown that the interaction term remains unchanged with changing $B_\parallel$ and has little dependence upon effective mass. Further, the effect of the Hartree term may be limited by considering a gate voltage and field regime in which only one subband is occupied. Note that the presence of an additional subband will affect both the Hartree and interaction terms, making an analysis

of the data more difficult. In this paper, values of the effective mass are deduced using the compressibility measurements where only a single subband is populated. The effective mass of the electron can therefore be determined from the gradient $\delta N_d/\delta N_p$.

4. Model and theory

In order to predict the effect of a parallel field on the coupled 2DEGs, the dispersion curves and Fermi surfaces at specific gate voltages were calculated by self-consistently solving the Schrödinger and Poisson equations for the structure. Many-body exchange and correlation interactions were approximated using the functional form proposed by Hedin and Lundqvist [22]. Although this has been shown to be quantitatively inaccurate [15, 20], qualitative trends may be modelled. The self-consistent potential $V(z)$, in the plane perpendicular to the 2DEGs, was fed into the Hamiltonian (equation (4) below), where the in-plane field was set parallel to the y-axis. Equation (4) was then solved for all points in k_x and k_y. This semi-classical approach is appropriate for non-zero $B_\parallel$ and low $B_\perp$ where a large number of LLs are present.

$$H(B_\parallel) = (p_y + eB_\parallel z)^2/2m^* + p_x^2/2m^* + p_z^2/2m^* + V(z). \tag{4}$$

The theoretical results for the sample, with no parallel field component, are shown in figure 2. Figure 2(a) shows the energy difference between the first and second subband levels with a minimum difference occurring at a gate voltage of -0.18 V when the two 2DEGs are on resonance. Note that the corresponding coupling energy is sufficiently large that the second subband is depopulated for a wide range of gate biases about resonance and only the symmetric wavefunction is populated at resonance (figure 2(b)). From the simulation, the symmetric–antisymmetric energy gap (Δ_{SAS}) of the strongly coupled 2DEGs was calculated to be 5 meV (see figure 2(a)), whilst the lower 2DEG was indeed decoupled with Δ_{SAS} equal to 5 μeV.

In figure 3, the calculated dispersion curves and Fermi surfaces are shown for two gate voltages: (a) $+0.16$ V and (b) -0.10 V. At $B_\parallel = 0$ T the dispersion curves for the upper (dashed line) and lower (solid line) subbands are both centred upon $k_x = 0$. The two curves, therefore, do not intersect and the number of populated subbands simply depends upon the position of the Fermi energy (E_F). As $B_\parallel$ is increased, the dispersion curves are displaced relative to each other in the k_x direction. Where the dispersion curves would intersect each other, the coupling results in an anticrossing. The effect of this anticrossing depends upon the subband densities. Considering a front gate voltage of $+0.16$ V (figure 3(a)), we see that the Fermi surface distortions can lead to the population and depopulation of subbands. At low fields ($B_\parallel = 3$ T) two subbands are occupied. As the parallel field is increased ($B_\parallel = 7$ T) the anticrossing of the dispersion curves moves the bottom of the higher-energy subband above the Fermi energy, depopulating this subband. At higher fields ($B_\parallel = 11$ T) the anticrossing point occurs at energies greater than the Fermi energy and two undistorted Fermi surfaces are seen again. Note that at a lower gate voltage of -0.10 V (figure 3(b)), the Fermi energy is sufficiently small that only one subband is populated at $B_\parallel = 3$ T. As the parallel field is increased the Fermi surface is again distorted (i.e. $B_\parallel = 7$ T) by the anticrossing, but the subband occupancy is not altered. At higher fields ($B_\parallel = 11$ T) the anticrossing point occurs at energies greater than the Fermi energy and a single, undistorted Fermi surface returns. The curvatures of the dispersion curves at the Fermi energy change as $B_\parallel$ increases, altering the effective mass. From the calculated dispersion curves, these effective mass changes can be determined. At high fields (~ 11 T) in our sample, the

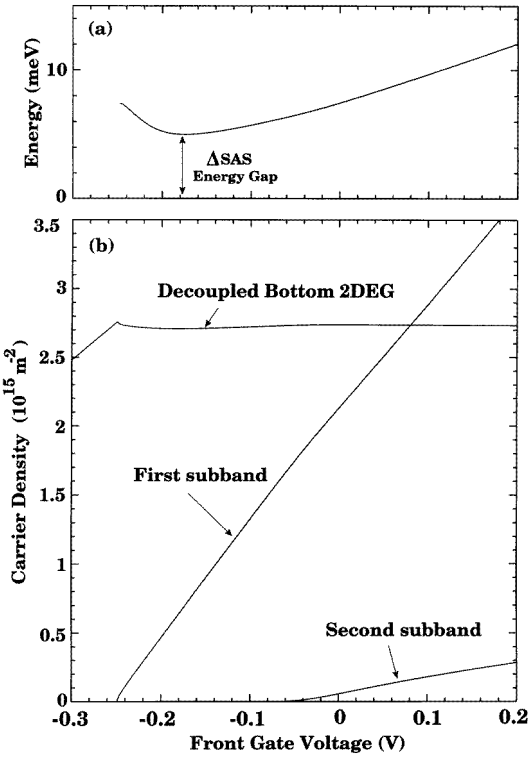

Figure 2. (a) The energy difference between the first two coupled subbands showing that the anticrossing of the energy levels has depleted the second subband at resonance; (b) the calculated carrier densities for the device as a function of applied gate bias.

anticrossing distortions do not affect the Fermi surfaces, and the effective mass would, therefore, be the same as at zero parallel field.

5. Results and discussion: magneto-transport

The longitudinal resistance of the sample was measured as a function of both gate bias and parallel field for constant perpendicular fields of 0.3 T (figure 4) and 1.0 T (figure 5). With sufficiently low perpendicular fields, $B_\perp = 0.3$ T, the LL related magneto-oscillations are obscured by thermal and scattering disorder and the dominant resistance features are due to a magneto-resistance resulting from each subband being depleted. The resistance minima correspond to the points at which a subband stops conducting [23, 24], and generally occur at a small finite carrier density, $\sim 3 \times 10^{14}$ m^{-2}, due to disorder. At $B_\parallel = 0.5$ T the first subband is populated at gate voltages greater than -0.25 V and a second subband is populated at gate biases greater than -0.04 V. Below -0.25 V the bottom, uncoupled, 2DEG is depleted by the front gate. With an increasing parallel field, the changing dispersion anticrossing moves the point at which the second subband becomes populated to more positive gate biases.

As $B_\parallel$ is increased further, the point at which the second subband is populated moves out of the available gate bias range. A second feature, however, is seen at much lower biases of around -0.14 V, indicating that a second subband is again being populated. A

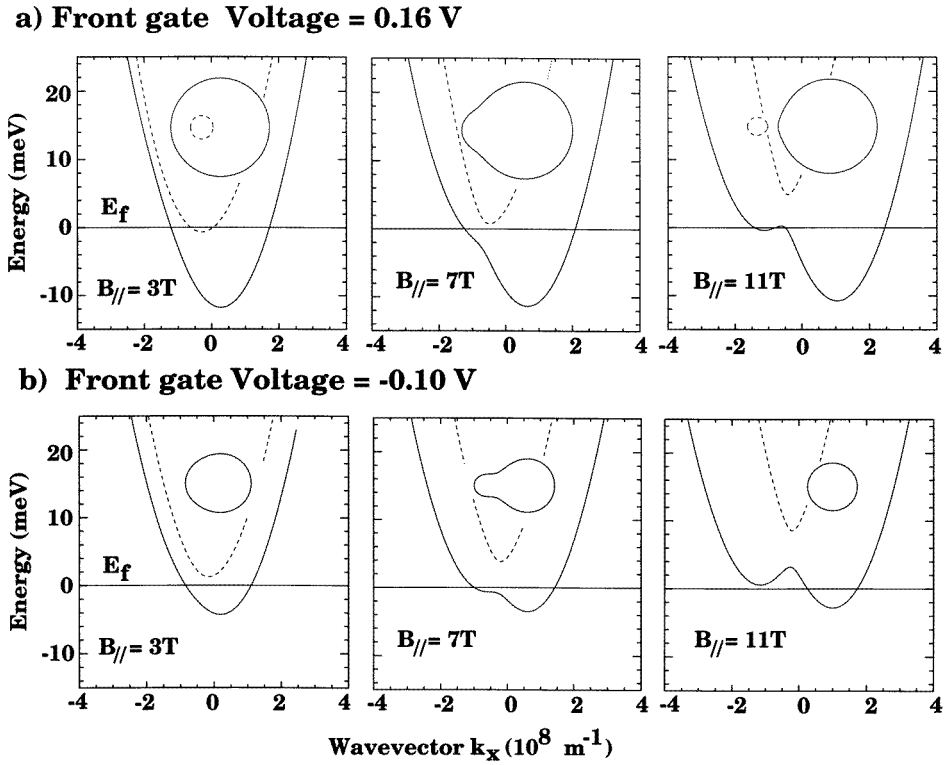

Figure 3. The calculated dispersion relations and Fermi surfaces for two different gate voltages, (a) +0.16 V, showing a 2–1–2 subband transition with increasing parallel field, and (b) −0.10 V, showing a single subband at all parallel fields.

similar feature can be seen in the data taken with a perpendicular field of 1.0 T (figure 5). In this case the resistance has been filtered to remove the magneto-resistive background component and emphasize the magneto-oscillations from the LLs. As each spin degenerate LL is occupied the density changes by $2eB_{\perp}/h$ carriers. The oscillations can, therefore, be used to map out the constant-density contours as the parallel field is increased. If the subbands are decoupled, or there is only one subband in the system, then the parallel field does not alter the subband densities and the magneto-oscillations should remain unaffected by the parallel field. This may be seen, for example, at low fields with gate voltages less than 0 V. Note that density changes due to diamagnetism are very small and may be considered as negligible. In contrast, at low parallel fields and gate voltages greater than 0 V, the parallel field changes the occupancy of the two subbands. In this case the magneto-oscillations shift in gate voltage as the parallel field is increased, reflecting the changing subband densities. Also seen in figure 5, as indicated by the broken line, there is a second transition at high parallel fields. This is accompanied by a suppression of the magneto-oscillations that may be related, using equation (1), to an increase in the electrons' effective mass. The temperature dependence of these magneto-oscillations can used to determine the electrons' effective mass, as discussed later. The subband transitions determined from the data of figures 4 and 5 are summarized in figure 6, where the positions at which the subbands populate have been plotted as a function of gate bias and parallel field and are in qualitative agreement with theory. The insets show, schematically, the dispersion relations in the different parallel

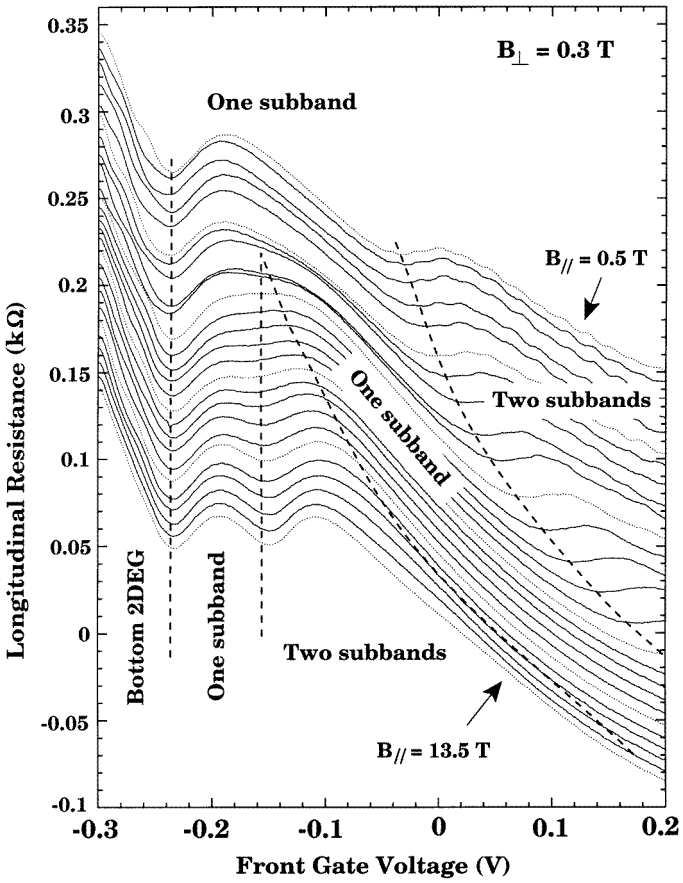

Figure 4. The longitudinal resistance measured as a function of applied gate bias at a fixed perpendicular field of 0.3 T and parallel fields from 0.5 to 13.0 T in 0.5 T steps. The magneto-resistance features due to the depletion of subbands are clearly seen and are labelled. The sample temperature was 1.5 K and the traces are offset vertically for clarity.

field regimes and were deduced from theoretical calculations (see section 4). We should add that the observed voltages at which the subband transitions occur are unaffected by the presence of LLs for the experimentally used perpendicular fields ($B_\perp \leqslant 1.0$ T).

Figure 7 shows the conductance as a function of gate bias with $B_\parallel = 0$ T and $B_\perp = 1.0$ T for twenty temperatures between 1.5 and 5.0 K. Comparing (a) the conductance determined from the experimental resistivities and (b) the same data filtered, the filtering is shown to remove effectively the magneto-resistive background. The magneto-oscillations are then seen to be symmetric about zero. The biases at which the subband transitions occur are apparent as the conductance increases in a steplike manner and the magneto-oscillations abruptly change amplitude. Similar data were collected for parallel fields up to 13 T. The mass ratios determined from the fitting procedures are shown in figure 8. For gate biases less than -0.22 V, the measured effective mass is that of the bottom, uncoupled 2DEG which remains near unity for all $B_\parallel$, as expected. Within the bias region ($-0.3 < V_{fg} < -0.18$) the first subband begins to populate, confusing the assignment of the oscillations, and it is not possible to extract sensible data within this region. At biases greater than -0.18 V,

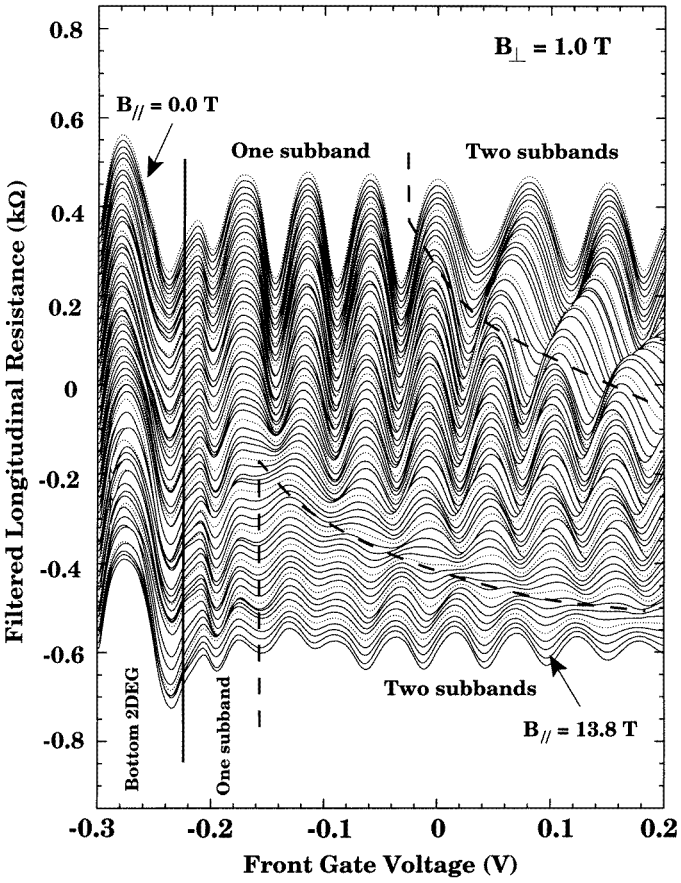

Figure 5. The longitudinal resistance measured as a function of applied gate bias at a fixed perpendicular field of 1.0 T and parallel fields from 0 to 13.8 T in 0.2 T steps. The data have been passed through a high-pass filter to remove the magneto-resistive background and highlight the suppression of the magneto-oscillations at high $B_{\|}$. The sample temperature was 1.5 K and the traces have been offset for clarity.

the effective mass rises as the Fermi surface is distorted by the parallel field. The Fermi energy then passes through the gap edge and the mass reaches a maximum before abruptly falling to near unity as the Fermi surfaces are completely separated and a second subband is populated. The distortions of the Fermi surfaces due to the anticrossing now occur at a point above the Fermi energy and electrons effectively see undistorted Fermi surfaces once again.

6. Results and discussion: compressibility

Measurements of the carrier density in the uncoupled detector layer are shown in figure 9 for a range of parallel fields up to 13.7 T, from which the coupled layer's compressibility may be determined. In each case the Hall resistance has been measured at a perpendicular field of 0.2 T, which is low enough that the magneto-oscillations due to LLs are undeveloped at the sample temperature of 1.5 K. At $B_{\|} = 0.2$ T the measured density initially decreases

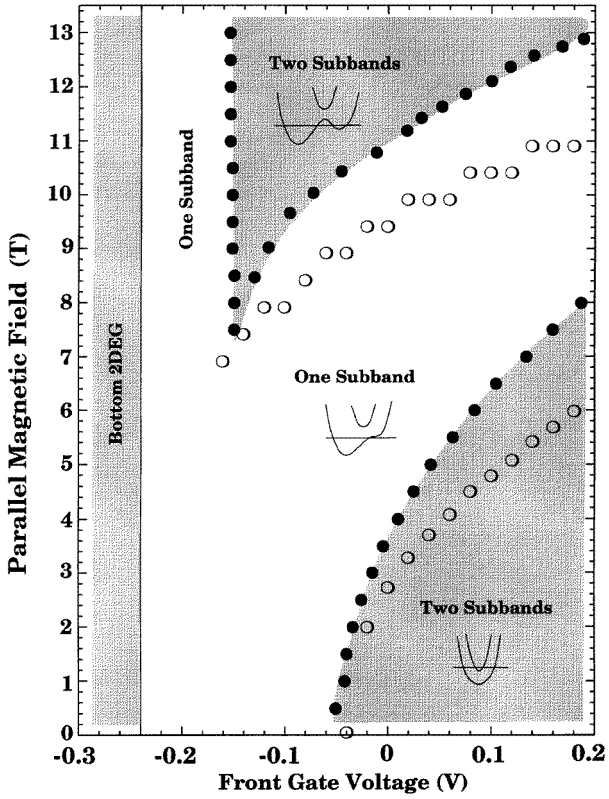

Figure 6. The experimentally determined population/depletion points of the subbands as a function of both gate voltage and parallel field, as determined from figures 2 and 3 (solid circles) and the subband population/depletion points as determined from the semi-classical calculation (empty circles). The inset figures show schematically the dispersion relations in the different regimes.

as carriers are added to the strongly coupled QWs because the negative interaction term within equation (4) dominates. With an increasing density in the coupled system, the negative terms become smaller and the positive kinetic term dominates. The measured density then increases until a second subband is populated. The detector 2DEG is then effectively screened from the front gate voltage by two subbands and the density changes in the detector layer are greatly reduced.

From these data the point at which the second subband becomes occupied can be identified and is seen to be in close agreement with the magneto-transport data. In the regions where a single subband is occupied, the rate of change of the detector layer carrier density (N_d) can be related to the chemical potential changes using equation (4). As seen in figure 9 the gradient ($\delta N_d/\delta N_p$) is a strong function of $B_\parallel$. In order to calculate the effective mass ratio (m^*/m_0), with respect to the effective mass at zero parallel field ($m_0 = 0.0667m_e$), one first extracts the gradient ($\delta N_d/\delta N_p$) at a fixed gate bias (fixed subband density) as a function of parallel field. We choose to evaluate the effective mass changes at a front gate bias of -0.07 V. At this bias, the compressibility is initially dominated by the kinetic energy and both the interaction and Hartree terms are comparatively smaller. To see how the interaction term varies with $B_\parallel$ one can look at the experimental regions in which the

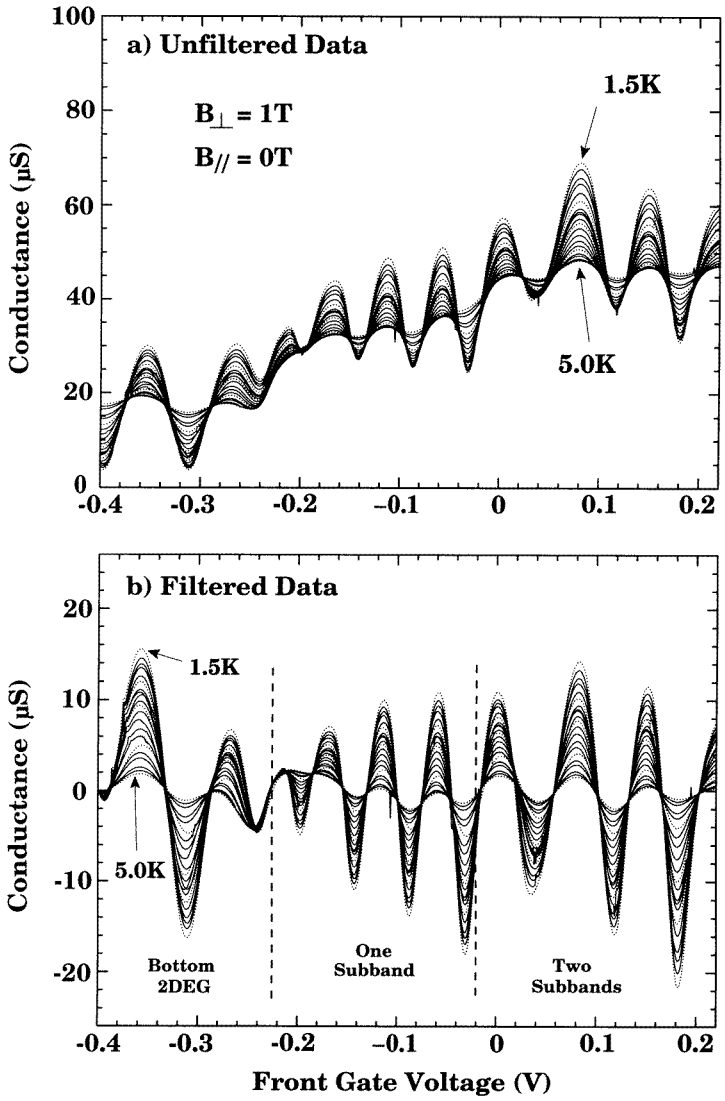

Figure 7. The temperature dependence of the magneto-oscillations as a function of gate bias with parallel and perpendicular field components of 0 and 1 T respectively. (a) The conductance, calculated using the tensor relationship $\sigma = \rho^{-1}$, for the temperature range 1.5–5.0 K. (b) The same data filtered to remove the magneto-resistive background. The gate voltages at which the different subbands are populated are indicated.

interaction term dominates (-0.2 V $< V_{fg} < -0.1$ V). With an increasing parallel field there are no significant changes in this region, indicating that the interaction term remains relatively constant with $B_{\|}$. Changes in the Hartree term can be determined from the model (section 4). This showed that the Hartree term has a contribution of less than 10% to the total $\delta N_d/\delta N_p$ for the gate voltage range (-0.18V$< V_{fg} < 0$ V). In order to minimize any further Hartree changes with in-plane field, we restrict ourselves to a field and gate voltage range in which the second subband remains unpopulated (0 T$< B_{\|} <$ 10 T).

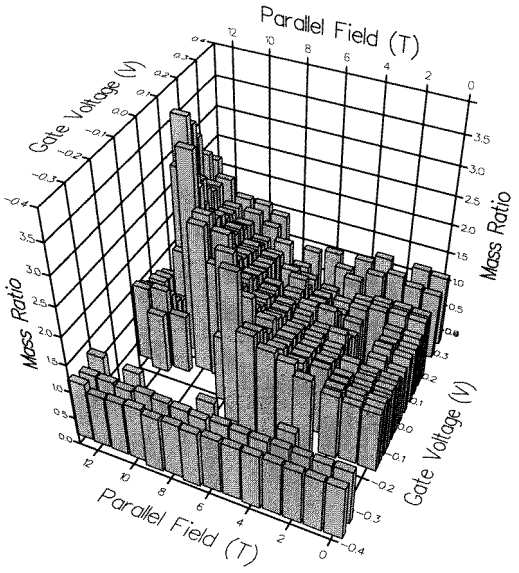

Figure 8. The effective mass ratio $m^*(B_\parallel)/0.0667m_e$, as determined from the temperature dependence of the magneto-oscillations, as a function of both parallel field and gate bias.

The other parameter required in the calculation is the distance d between the electrons in the detector and those in the strongly coupled DQW. The precise value of d will depend upon the electron wavefunctions, but calculations using the model allow an estimate for this value of 450 Å at $V_g = -0.07$ V. This corresponds to the majority of the coupled 2DEG wavefunction lying within the top QW. This is intuitively correct as both theoretically (figure 2) and experimentally (figure 6) the second subband, associated with charge lying mainly within the bottom well, is depopulated by the subband anticrossing at this gate voltage.

Figure 9 shows the effective mass evaluated at a gate bias of -0.07 V as a function of $B_\parallel$. As a comparison, the masses determined from the magneto-transport data are shown together with those calculated from the model. It can be seen that as $B_\parallel$ increases the mass rapidly rises as the Fermi surface is distorted by an in-plane field. At fields above 10 T a second subband becomes occupied and the density changes in the detector layer are greatly reduced. The compressibility results are in good agreement with both the magneto-transport data and the model, confirming that our interpretation of the compressibility data is correct. The largest source of errors in the compressibility effective masses is the estimate of the capacitive distance d. Errors in estimating d could be reduced in future measurements by using a wider spacer layer between the detector and probed coupled 2DEGs. This would, however, reduce the size of the carrier density changes in the detector 2DEG.

7. Analysis and conclusion

In figure 10, the effective mass ratio increases from unity at $B_\parallel = 0$ T to a maximum at ~ 10 T. At this field the mass then falls back to unity as the Fermi surfaces are decoupled by the parallel field. With the exception of the magnitudes of the in-plane fields, the theoretical masses for this subband follow the same trend as in both the experiments. Our

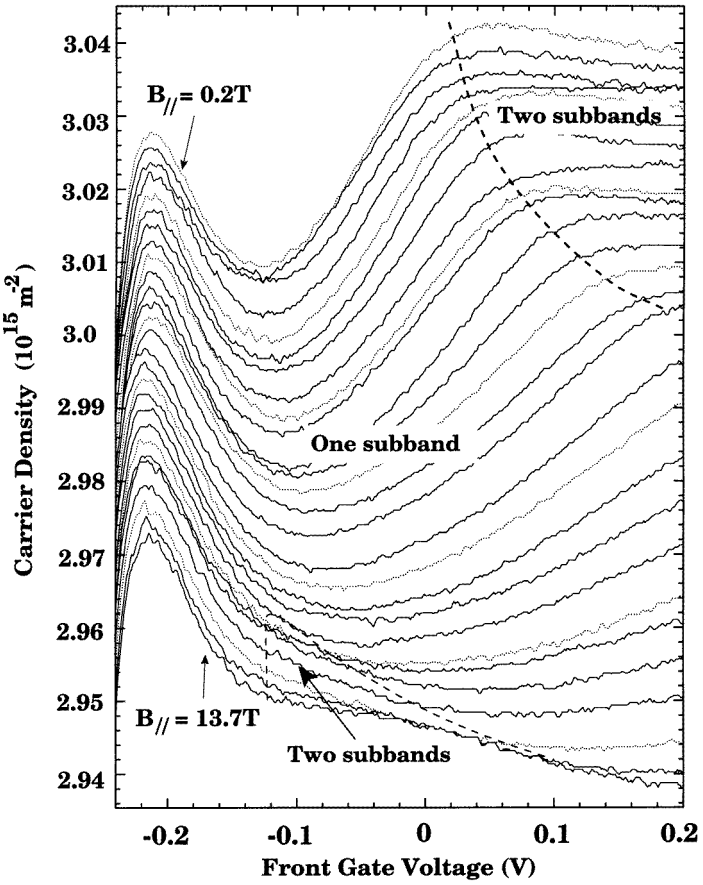

Figure 9. The carrier density of the independently contacted, decoupled, bottom 2DEG as a function of both gate bias and parallel fields up to 13.7 T. The regions of interaction dominated ($V_{fg} < -0.1$ V) and kinetic dominated ($V_{fg} > -0.1$ V) compressibility are clearly seen. The regions of different subband population are indicated and the curves are offset vertically for clarity. Measurements were made with a sample temperature of 1.5 K.

experimental effective masses may be compared with those of previous experiments [11] where the effective mass was determined from SdH oscillations in a tilted field rather than from gate bias sweeps. In [11], the effective mass of the second (lower-energy) subband was probed and was seen to initially decrease from unity with an increasing parallel field. At very high parallel fields the mass ratio was observed to return to unity as the two subbands decoupled. In our sample, the higher-energy subband has either too few carriers to generate magneto-oscillations or is rapidly depopulated by the in-plane field. Using our sample we are, therefore, able to probe the effective mass of the lower-energy subband. The observed changes in the effective mass agree with the prediction of Lyo *et al* [10] that this subband has an effective mass that *increases* with parallel field.

A noticeable feature of our data is that we only see magneto-oscillations due to the larger of the Fermi surface orbitals at *all* gate biases. One can see, though, from the model (figure 2) that the carrier density of the second subband varies very much more slowly than the first with gate voltage. Hence, over a given gate bias range, the number of LLs

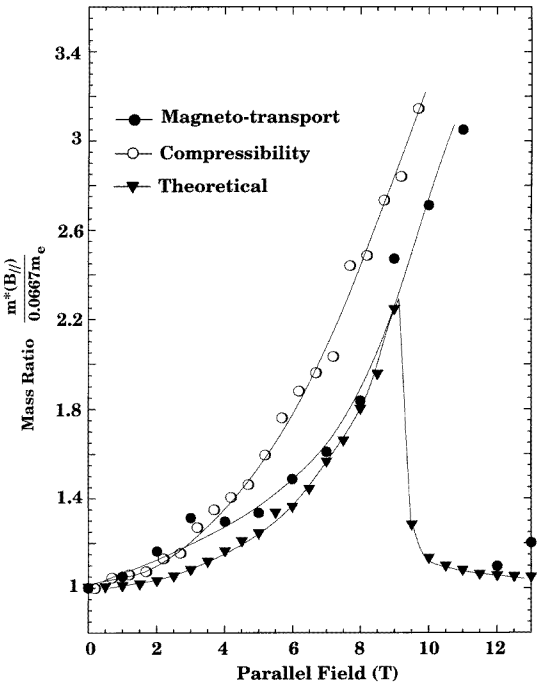

Figure 10. The effective mass ratio $m^*(B_\parallel)/0.0667m_e$ at a gate bias of -0.07 V as determined from the temperature dependence of the magneto-oscillations (solid circles), the compressibility data (empty circles), and the semi-classical calculation (triangles). Lines are included as guides to the eye only.

depopulated is very much less in the second subband than in the first subband. The period of the second-subband LL oscillations is very much larger than those from the first subband, therefore only the first subband is seen. At high $B_\parallel$ the two Fermi surfaces are 'decoupled' by the in-plane field. Once the first subband (closest to the gate) has been populated, this subband will screen the second from the applied bias. This will again result in the carrier density changes within the first subband being very much greater than those of the second, and only one oscillation being seen. The presence of a single-period oscillation in our data can thus be explained. In previous publications [10, 11], the observation of a single-period oscillation may be attributed to electrons being scattered out of large Fermi surfaces before completing an orbit, hence no magneto-oscillations would be seen for that subband.

It should be noted that the effective masses determined in magneto-transport and compressibility measurements would be expected to be slightly different. This is because a magneto-transport measurement requires the application of a quantizing perpendicular field component which will have some effect on both the effective masses and the subband populations. Indeed it can significantly alter the behaviour of the coupled 2DEGs [25, 26], although, within these experiments, no noticeable changes are apparent for the different perpendicular fields used. In addition, the transport experiment is orientation dependent [9]. In comparison, the compressibility measurements do not rely upon the formation of Landau levels, and will probe changes over the entire Fermi surface with no orientation dependence. The compressibility method, however, has the disadvantage that with more than one subband occupied the density changes within the detector layer are greatly reduced.

8. Summary

In summary, we have mapped out the population of the subbands in a strongly coupled 2DEG system as a function of density and parallel field using both magneto-resistance depletion and compressibility measurements. The results are shown to be in agreement with self-consistent calculations of the structure. In addition, we have determined the changes in the effective mass as the density and parallel field distort the Fermi surfaces. Large enhancements of the effective mass have been observed using both methods, and the results are shown to be in agreement with theory. By growing a decoupled 2DEG below the coupled 2DEGs, we demonstrate that non-invasive measurements of such properties as the effective mass and chemical potential changes within the coupled 2DEGs are possible. These techniques could be used to map out the effective mass and chemical potential changes within different systems.

Acknowledgments

The authors acknowledge the support of the UK Engineering and Physical Sciences Research Council. One of the authors, DAR, would like to acknowledge the support of Toshiba Cambridge Research Centre.

References

[1] Palevski A, Beltram F, Capasso F, Pfeiffer L and West K W 1990 *Phys. Rev. Lett.* **65** 1929
[2] Smoliner J, Gornik E and Weimann G 1989 *Appl. Phys. Lett.* **52** 2136
[3] Eisenstein J P, Pfeiffer L N and West K W 1992 *Phys. Rev. Lett.* **69** 3804
[4] Moon K, Mori H, Kun Y, Girvin S M, Macdonald A H, Zheng L, Yoshioka D and Zhangn S-C 1995 *Phys. Rev.* B **51** 5138
[5] Yoshioka D, Macdonald A H and Girvin S M 1989 *Phys. Rev.* B **39** 1932
[6] Boebinger G S, Murphy S Q, Eisenstein J P, Pfeiffer L N, West K W and Song H 1994 *Surf. Sci.* **305** 8
[7] Suen Y W, Engel L W, Santos M B, Shayegan M and Tsui D C 1992 *Phys. Rev. Lett.* **68** 1379
[8] Millard I S, Patel N K, Simmons M Y, Hamilton A R, Ritchie D A and Pepper M 1996 *J. Phys.: Condens. Matter* **8** L311
[9] Kurobe A, Castleton I M, Linfield E H, Grimshaw M P, Brown K M, Ritchie D A, Pepper M and Jones G A C 1994 *Phys. Rev.* B **50** 4889
[10] Lyo S K 1995 *Phys. Rev.* B **51** 11 160
[11] Simmons J A, Hariff N E and Klem J F 1995 *Phys. Rev.* B **51** 11 156
[12] Leadley D R, Nicholas R J, Harris J J and Foxon C T 1990 *20th Int. Conf. on Physics of Semiconductors (Thessaloniki, 1990)* ed E M Anastassakis and J D Joannopoulos (Singapore: World Scientific) p 1609
[13] Boebinger G S, Passner A, Pfieffer L N and West K W 1991 *Phys. Rev.* B **43** 12 673
[14] Eisenstein J P, Pfeiffer L N and West K W 1992 *Phys. Rev. Lett.* **68** 674
[15] Millard I S, Patel N K, Simmons M Y, Linfield E H, Ritchie D A and Pepper M 1996 *Appl. Phys. Lett.* **68** 3323
[16] Patel N K, Millard I S, Linfield E H, Rose P D, Ritchie D A, Jones G A C and M P 1995 *J. Phys.: Condens. Matter* **7** L585
[17] Eisenstein J P, Pfeiffer L N and West K W 1994 *Phys. Rev.* B **50** 1760
[18] Ying X, Parihar S R, Manoharan H C and Shayegan M 1995 *Phys. Rev.* B **52** 611
[19] Eisenstein J P, Pfeiffer L N and West K W 1990 *Appl. Phys. Lett.* **57** 2324
[20] Millard I S, Patel N K, Foden C, Linfield E H, Simmons M Y, Ritchie D A and Pepper M 1996 *Phys. Rev.* B submitted
[21] Millard I S and Patel N K 1996 unpublished
[22] Hedin L and Lundqvist B I 1971 *J. Phys. C: Solid State Phys.* **4** 2064
[23] Kane M J, Apsley N, Anderson D A, Taylor L L and Kerr T 1985 *J. Phys. C: Solid State Phys.* **18** 5629
[24] Millard I S, Patel I S, Linfield I S, Rose P D, Simmons M Y, Ritchie D A, Jones G A C and Pepper M 1996 *Semicond. Sci. Technol.* **11** 483

[25] Hu J and Macdonald A H 1992 *Phys. Rev.* B **46** 12 554
[26] Harff N E, Simmons J A, Boebinger G S, Klem J F, Pfeiffer L N and West K W 1996 *Proc. 23rd ICPS (Berlin, 1996)* vol 3, ed M Scheffler and R Zimmerman (Singapore: World Scientific) p 2199